Supplemental Information for Marrero et al. 2018: Controls on subaerial erosion rates in Antarctica

1. Sample Collection

The samples were collected during two consecutive field seasons in Antarctica (2012/2013 & 2014). Bedrock samples were collected from many areas within the Marble Hills. All samples were collected as thin pieces or chips from the surface of carbonate bedrock. Samples referred to as 'qualitative' indicate the first batch of samples, which did not include sufficient carrier and caused them to be out of the calibrated measurement range for the AMS. These samples are excluded from all analyses although they are included here and in the Supplementary Spreadsheet.

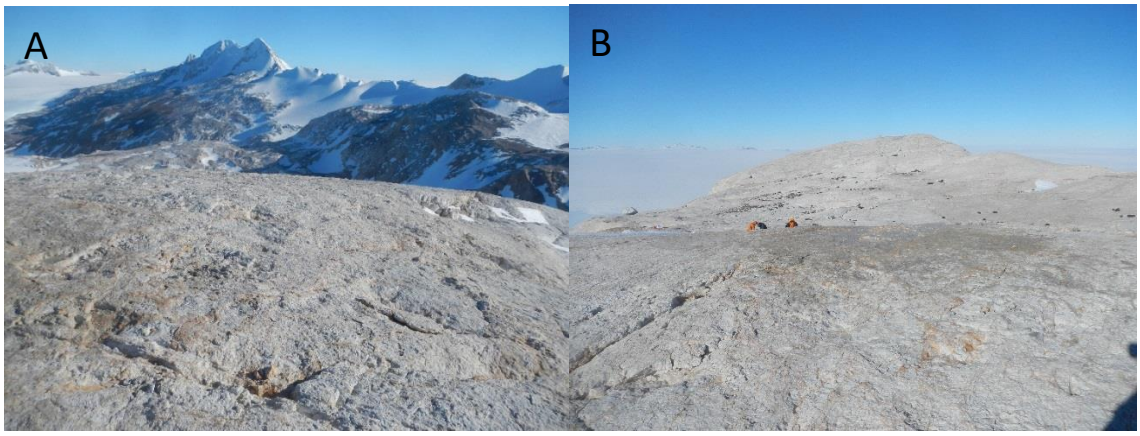

Figure S1 – MH12-30/MH12-31 (Marble Dome).

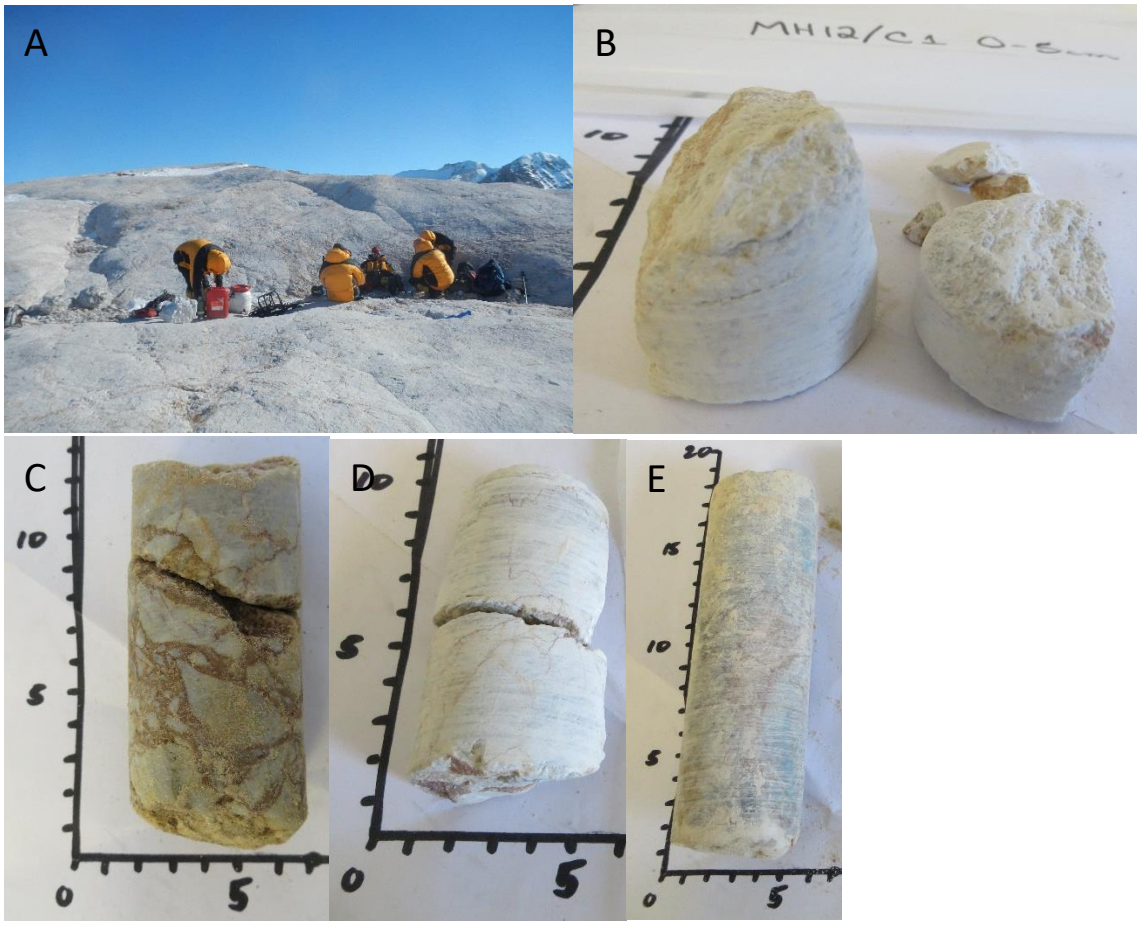

Figure S2 – MH12-Core (Marble Dome). The 1.6 m core was drilled at the highest point visible (above the people) on the ice-moulded bedrock in the foreground. Several MH12 core sections are shown, including 0-5 cm (processed), 95-105 cm, 126-130 cm, and 132-149 cm.

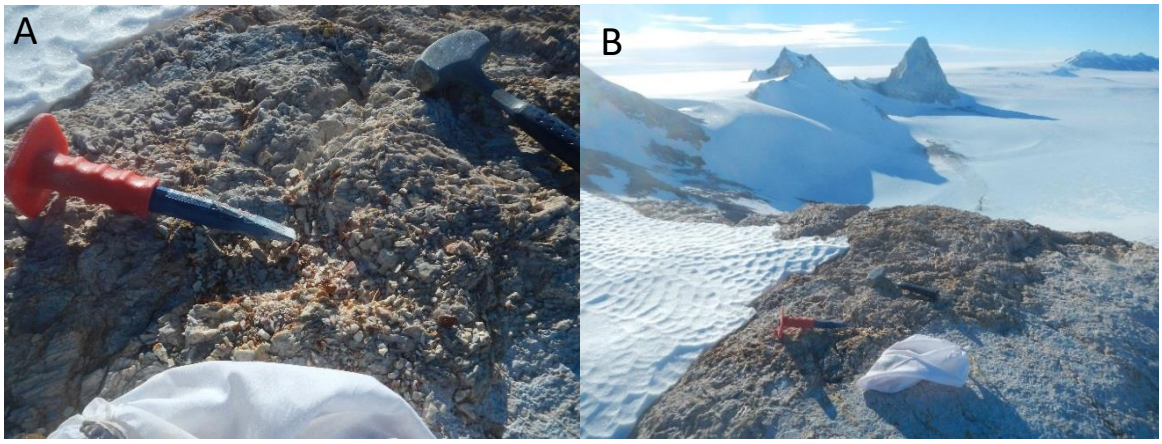

Figure S3 - MH12-32 (Marble Dome). Calcite vein.

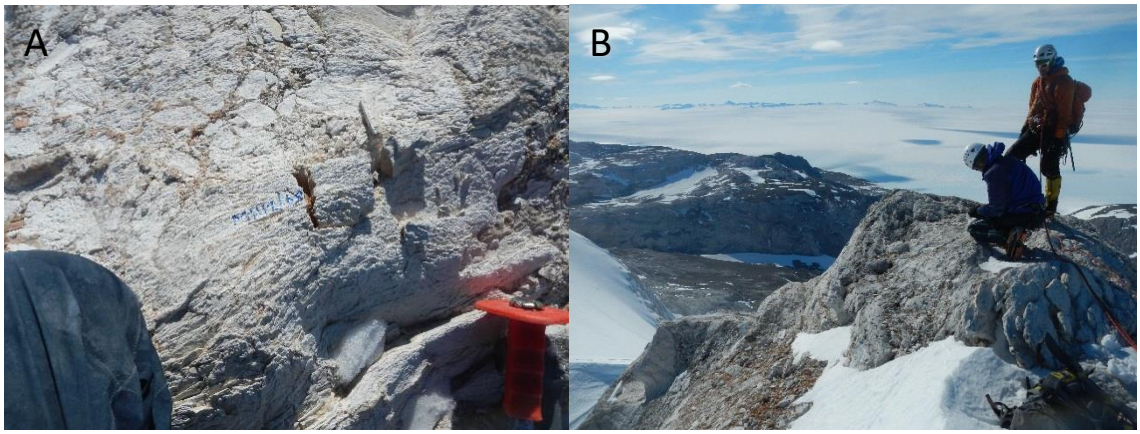

Figure S4 - MH12-68 on Mt. Fordell. Qualitative samples MH12-69 and MH12-70 were also collected from this location.

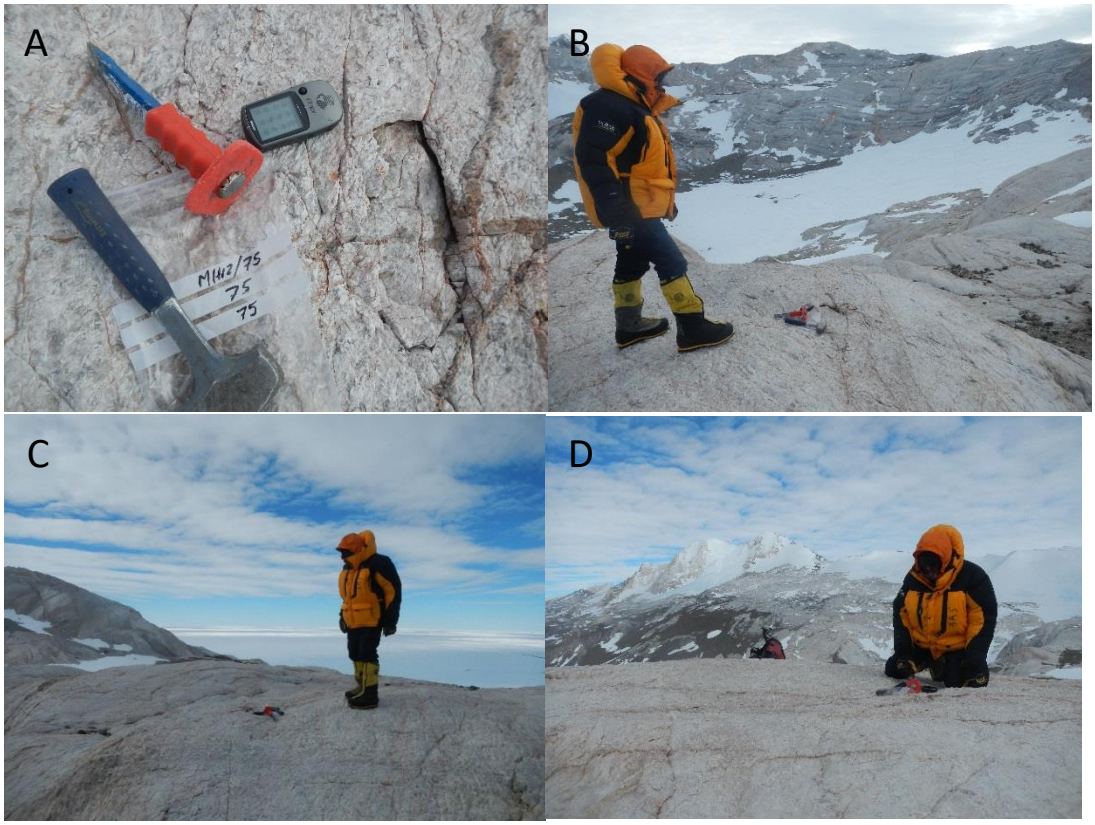

Figure S5 - MH12-75 (Complex exposure area).

Figure S6 - MH14-13 (Complex exposure area)

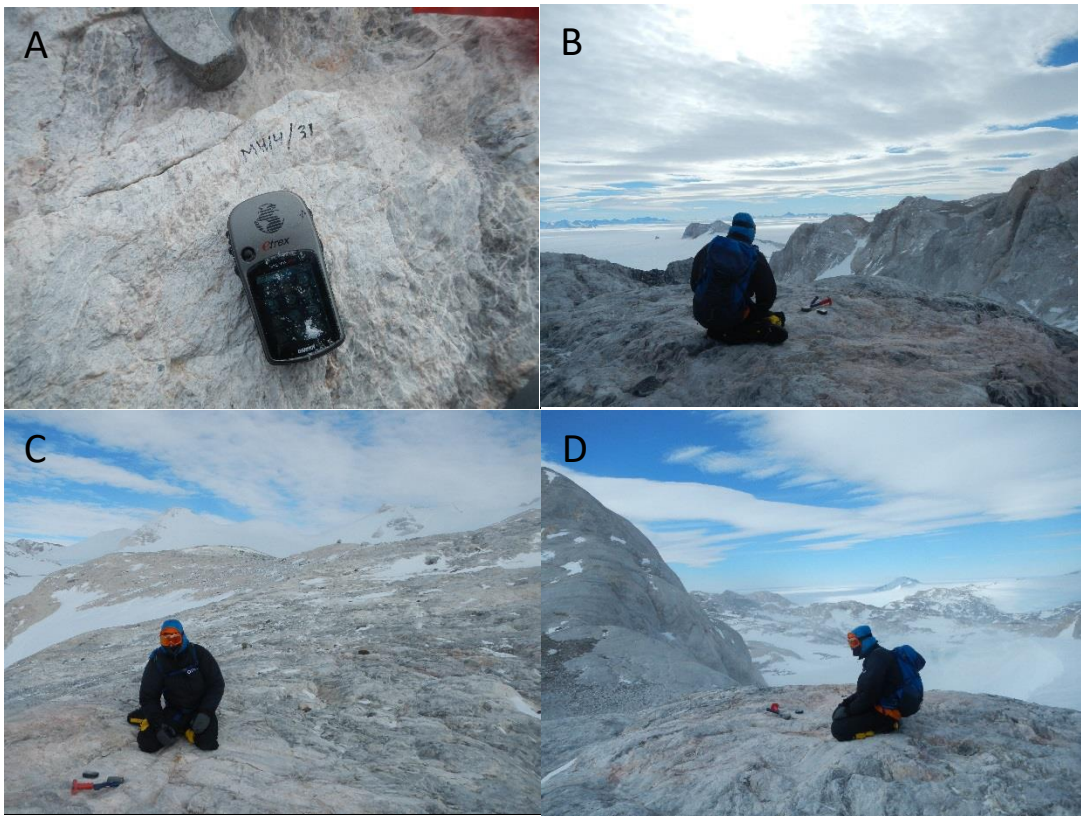

Figure S7 - MH14-31 (Complex exposure area)

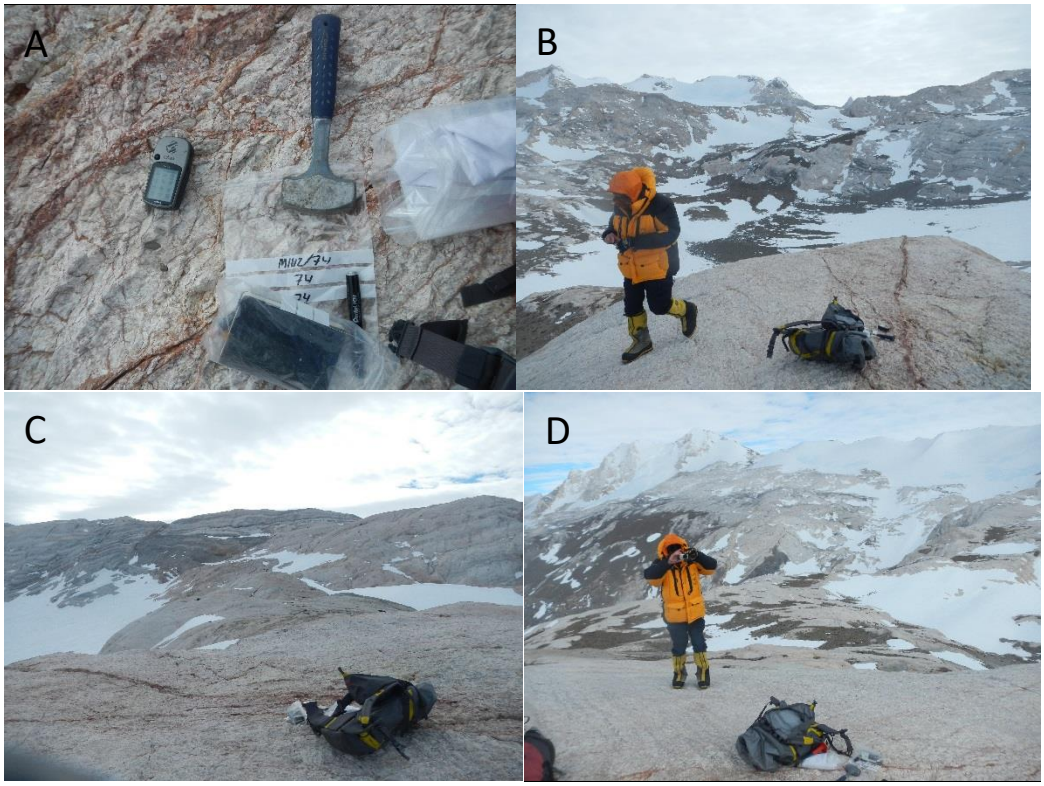

Figure S8 - MH12-74 (Qualitative sample; Complex exposure area)

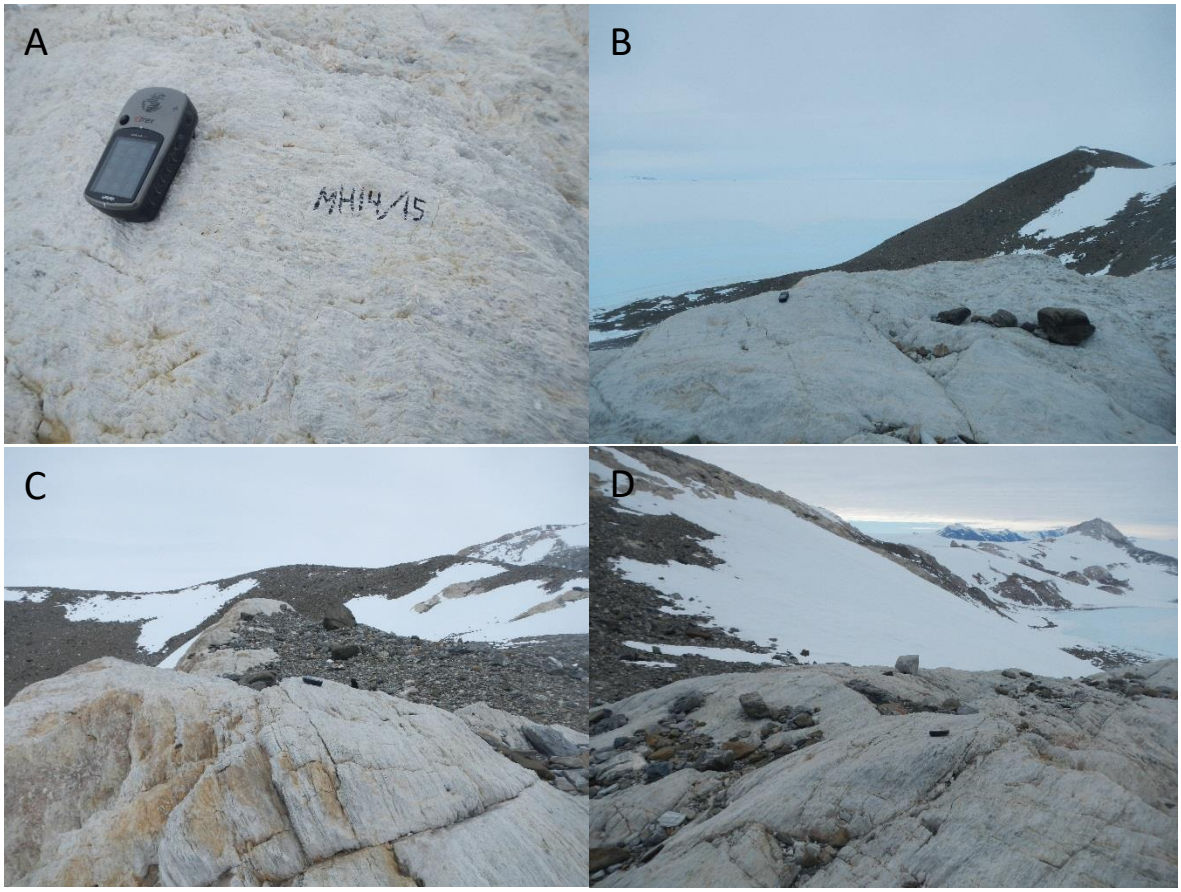

Figure S9 - MH14-15.

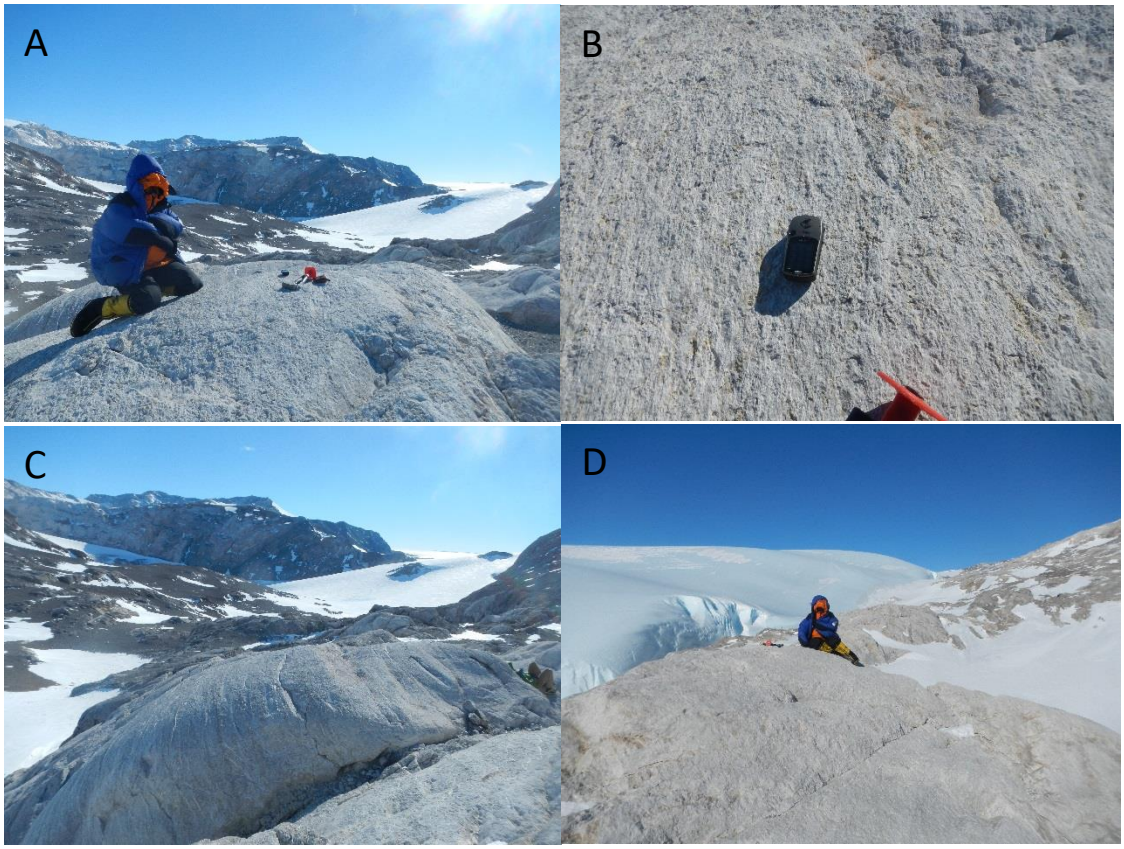

Figure S10 – MH14-38

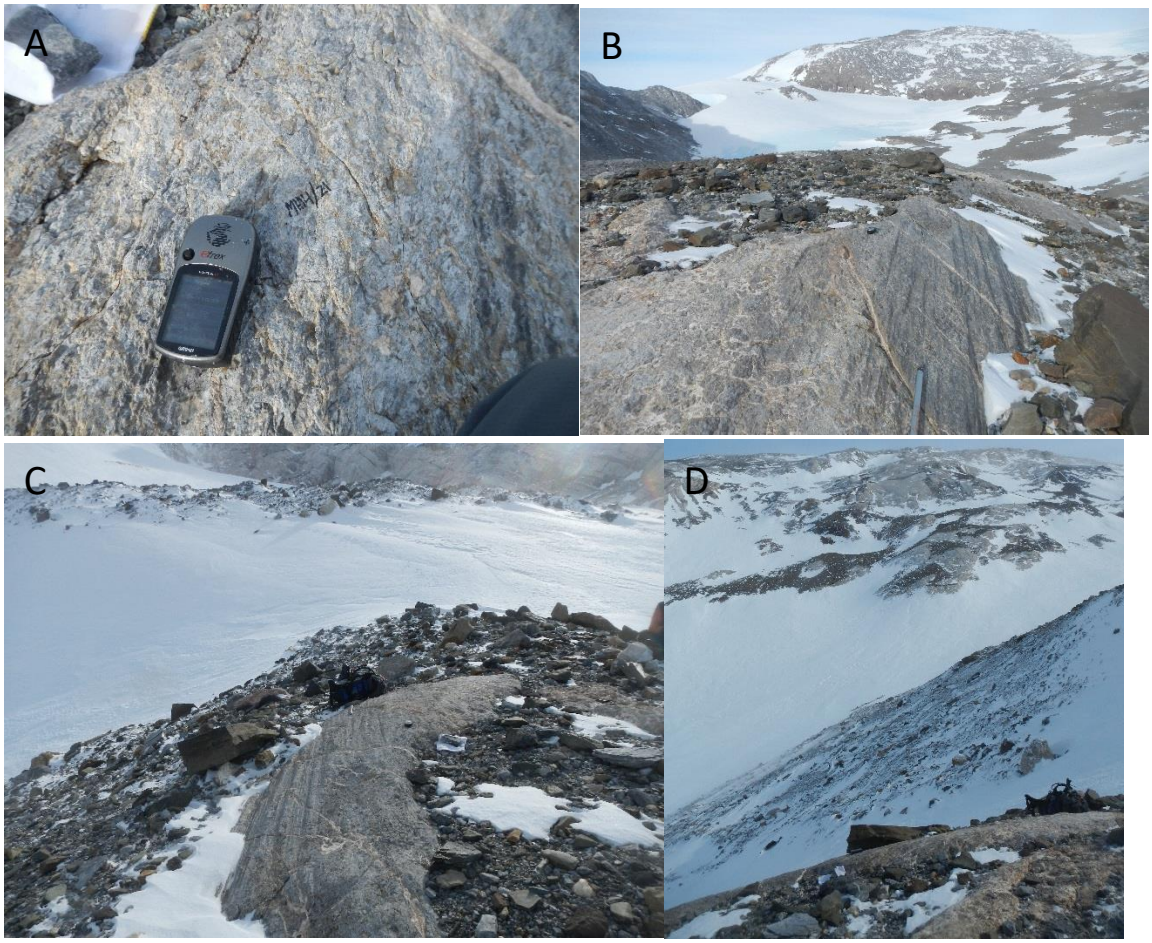

Figure S11 – MH14-21

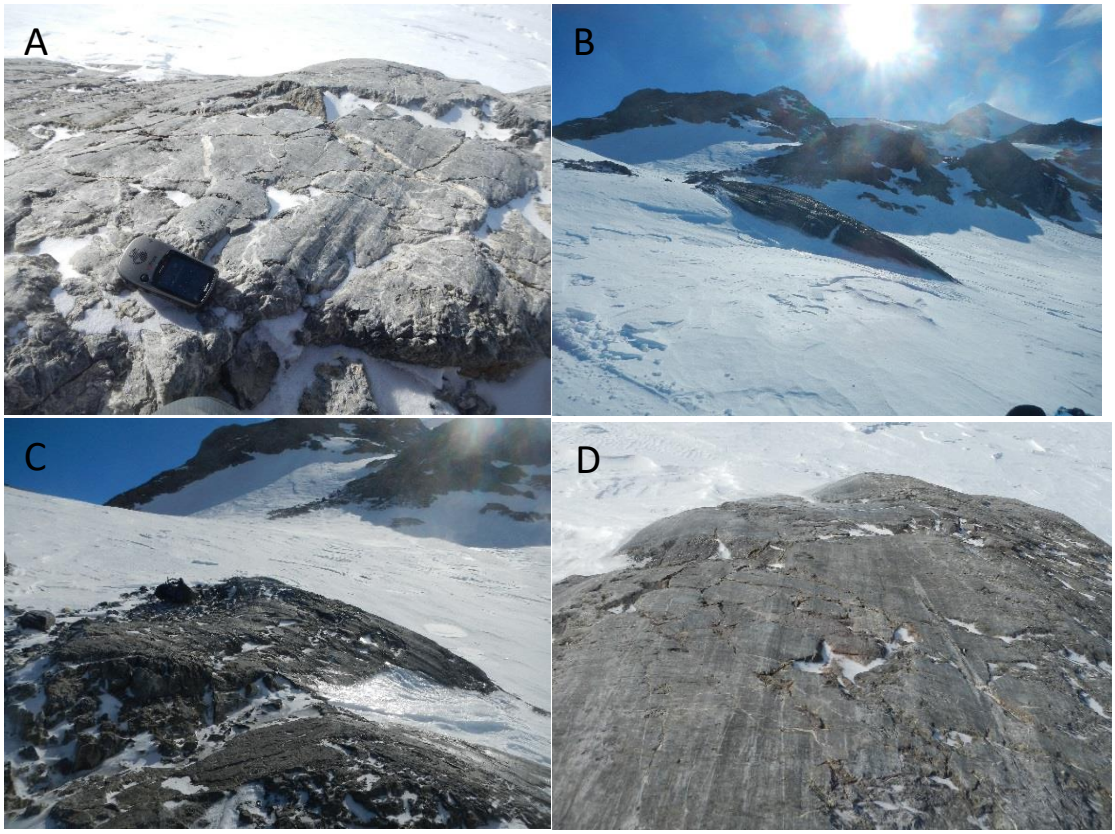

Figure S12 – MH14-37

2. Sample Processing

The samples were processed at the University of Edinburgh cosmogenic nuclide lab. The processing at University of Edinburgh is detailed below.

Detailed sample photos were taken in the lab. All samples were thin enough that they were not trimmed prior to crushing. Crushing was performed in a jaw crusher first and then finished in a small disk mill. Samples were crushed until most of the sample was 210-750 micrometers. The samples were split using the cone-and-quarter method to obtain both the sample and a quantitative sample for XRF analysis of the bulk rock. The fractions <210 and >750 microns were also split and combined in appropriate amounts so the entire rock was represented in the XRF sample. Due to the very low Cl contents of the samples, only a couple of bulk rock composition samples were done for each rock type and then those average results were used for all similar samples. The composition of the rock is similar across lithologies and choice of bulk/trace composition does not significantly affect the results. The XRF analyses were performed at the University of Edinburgh. ICP-OES and neutron activation (B only) were performed at SGS Mineral Services, Inc. (Toronto, Canada). Density was not measured and was assumed based on averages for the rock type and was given a larger uncertainty to account for this.

The sample was placed in an HDPE plastic single-use bottle and etched with small amounts of dilute nitric acid until approximately 20-30% of the sample material had been removed. The samples were dried in the oven and then weighed into new, water-washed plastic bottles for dissolution. Sample amounts varied between 0.5 g and 5 g for quantitative samples and ~30 g for qualitative samples, with ~1.5-5 mg of ^{35}Cl carrier (ORNL, batch 150301). Pure carrier solution was mixed with Fisher NaCl to achieve a final ^{35}Cl/^{37}Cl carrier ratio of approximately 20. The samples were dissolved

by repeatedly adding small amounts of 2M nitric acid over several hours (covered between additions). When the samples were completely dissolved, they were centrifuged into water-washed disposable plastic centrifuge tubes. The undissolved material was dried, weighed, and subtracted from the sample size.

The target material, AgCl, was precipitated using AgNO3 added to the warm sample solution and allowed to cool and settle overnight. The AgCl was purified through dissolution and reprecipitation. Sulphur was removed using a week-long removal step using BaNO3. The samples were rinsed, dried, pressed into copper cathodes, and measured at the AMS facility at SUERC. For any further details about the laboratory procedure, contact Shasta Marrero, Andy Hein (andy.hein@ed.ac.uk), or the laboratory manager at the University of Edinburgh cosmogenic nuclide lab.

The ^{36}Cl and total Cl were calculated from the AMS results using the method used by the Purdue PRIME Lab (Marc Caffee and Greg Chmiel, pers. communication, 7 April 2018), which is based on the principles in Faure (1987). This gives nominal results similar to the results calculated using Wilcken et al. (2013). However, the blank subtraction assumptions made by Purdue more closely resemble our method, so the uncertainties from this method were adopted to calculate the final values.

Blank subtractions for total Cl were generally small (<5%), although up to 12% for very low-Cl samples. Blank subtractions for 36Cl concentrations were <0.5% for most samples, although slightly larger for the lower elevation samples with lower concentrations. Sample concentrations were corrected using process blanks processed at the same time as the samples as well as pure spike blanks processed separately. ^{36}Cl concentrations were blank-corrected on a per batch basis. The supplemental spreadsheet has the original AMS results and blank subtraction information for each sample.

Sample erosion rates can be calculated with varying degrees of uncertainty. For comparison, these samples have been run with full uncertainties (external) as well as a reduced uncertainty (production rate uncertainty and AMS uncertainty only). The batch of samples that were out of range when measured using AMS are being used in a qualitative fashion only. Erosion rate results from these qualitative samples and the different uncertainty comparisons for the main samples are all included in the Supplemental Spreadsheet, with additional information that would be needed to recreate these results (e.g. original AMS results, composition, sample mass).

3. Erosion rate calculations

For stable nuclides (^{3}He and ^{21}Ne), CRONUScalc assumes steady-state via long-term exposure and solves Equation S1 (Equation 4.26 in Dunai (2010); originally from Lal (1991)) for the erosion rate (ε), using the given density (ρ), the measured nuclide concentration (C_{total}), and the attenuation length (Λ_i) calculated by CRONUScalc. The production rates (P_i) are discussed explicitly in the next section. This equation has been simplified because only one production pathway (spallation) was considered and only at the surface. This method only applies to stable nuclides and is only applicable for Lal/Stone time-independent scaling.

$$C_{total} = \sum_i \frac{P}{\rho\varepsilon/\Lambda} \qquad \text{Eqn S1}$$

For all other nuclides, erosion rates were calculated by assuming an infinite age for the sample (>> 6 half-lives) and then iteratively changing erosion rate and predicting the resulting nuclide concentration until the predicted concentration matched the observed value. This method is applicable to all unstable nuclides and for all scaling models.

Most production rates used in the default version of CRONUScalc were calibrated as part of the CRONUS-Earth Project and can be found in Borchers et al. (2016) for the spallation production rates, Phillips et al. (2016) contains the uncertainties on the production rates as well as muon calibration information for 26Al and 10Be, Marrero et al. (2016) for all values pertaining to ^{36Cl}.

Ne was added to the CRONUScalc code and was modelled was modelled after the existing code for ^{3}He and only includes spallation production. The ^{21}Ne production rate is tied to the total CRONUScalc ^{10}Be production rate (assuming 1.5% production from muons[49]) with a ^{21}Ne/^{10}Be ratio of 4.08 ± 0.37[48], resulting in a ^{21}Ne production rate of 16.26 ± 1.96 atoms $g^{-1}a^{-1}$ at sea level, high latitude scaled according to nuclide-dependent Lifton-Sato-Dunai model (Balco and Shuster, 2009; Borchers et al., 2016; Lifton et al., 2014). There are several other alternative ^{21}Ne production rates (all converted to be consistent with Lifton-Sato-Dunai scaling): 14.5 (Amidon et al., 2009), 18.0 (Vermeesch et al., 2009), and 18.9 (Niedermann et al., 1994). The Balco and Shuster[48] rate was used because it is based on ratios tied to ^{10}Be instead of ^{26}Al, it uses a relatively large dataset compared to other ^{21}Ne studies, it was performed using Antarctic samples, and the resulting rate falls in the middle of the production rate range. These results compare well with the new Version 3 calculator (https://hess.ess.washington.edu/) results for ^{21}Ne. We use the results from this modification to remain internally consistent with production calculations.

Although many previous comparisons of erosion rate results were limited to a single nuclide (cf. Portenga and Bierman, 2011), additional nuclides are necessary for representation from non-quartz-bearing lithologies. CRONUScalc was used to calibrate across multiple nuclides in the original calibration, including multiple nuclides in the same quartz splits (Al, Be, 14C) and He and Cl in the same basalt flows, so there is no reason to doubt internuclide comparisons. Figure S13 shows the comparison of results from different nuclides for individual samples. Although there were systematic offsets between Ne and Be for some studies, these were also noted by the original authors of the studies, so our results are consistent with the original findings. Figure S14 shows all the sandstone erosion rates broken down by nuclide. There is no statistically significant difference between the populations.

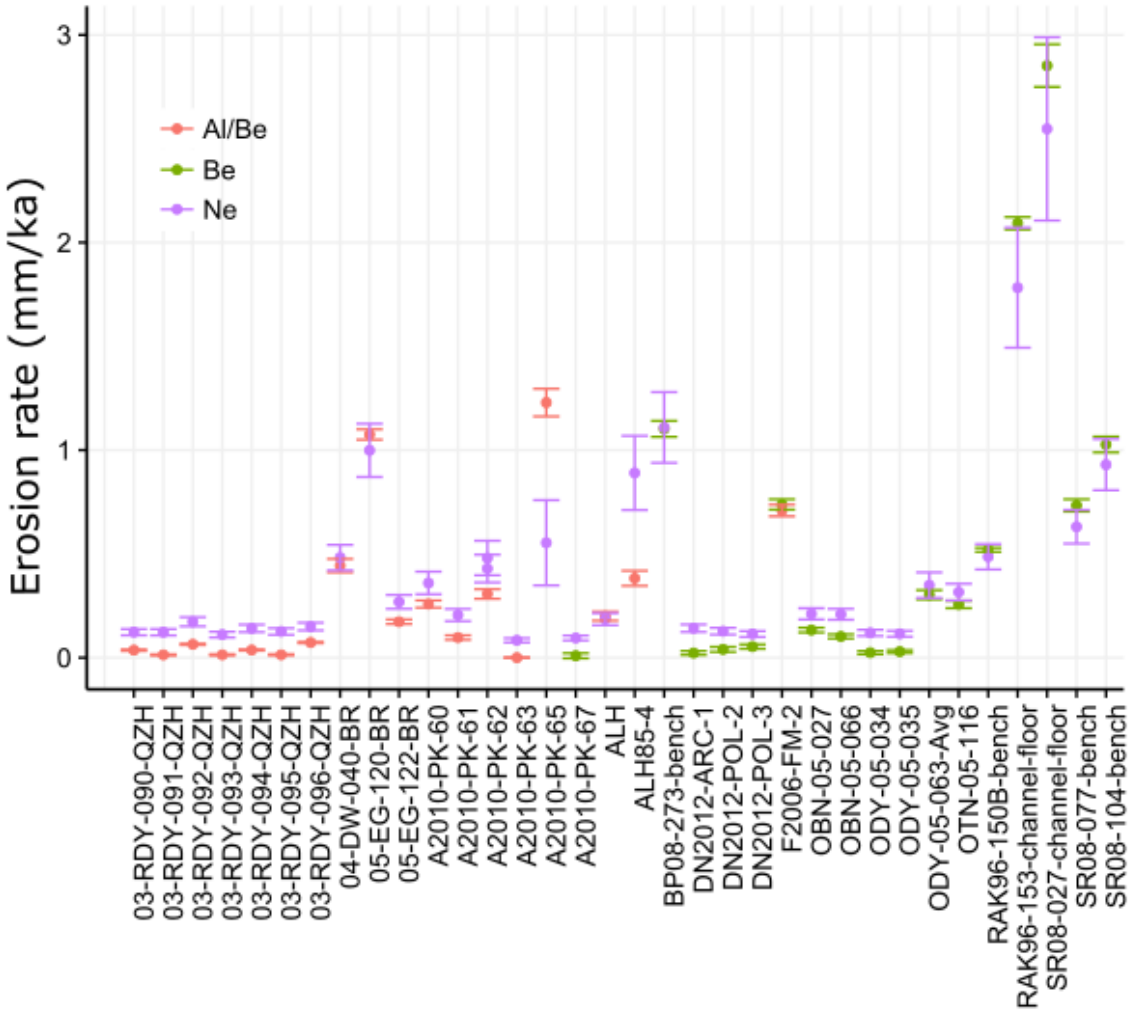

Figure S13 – Individual sample comparison of recalculated results for different nuclides.

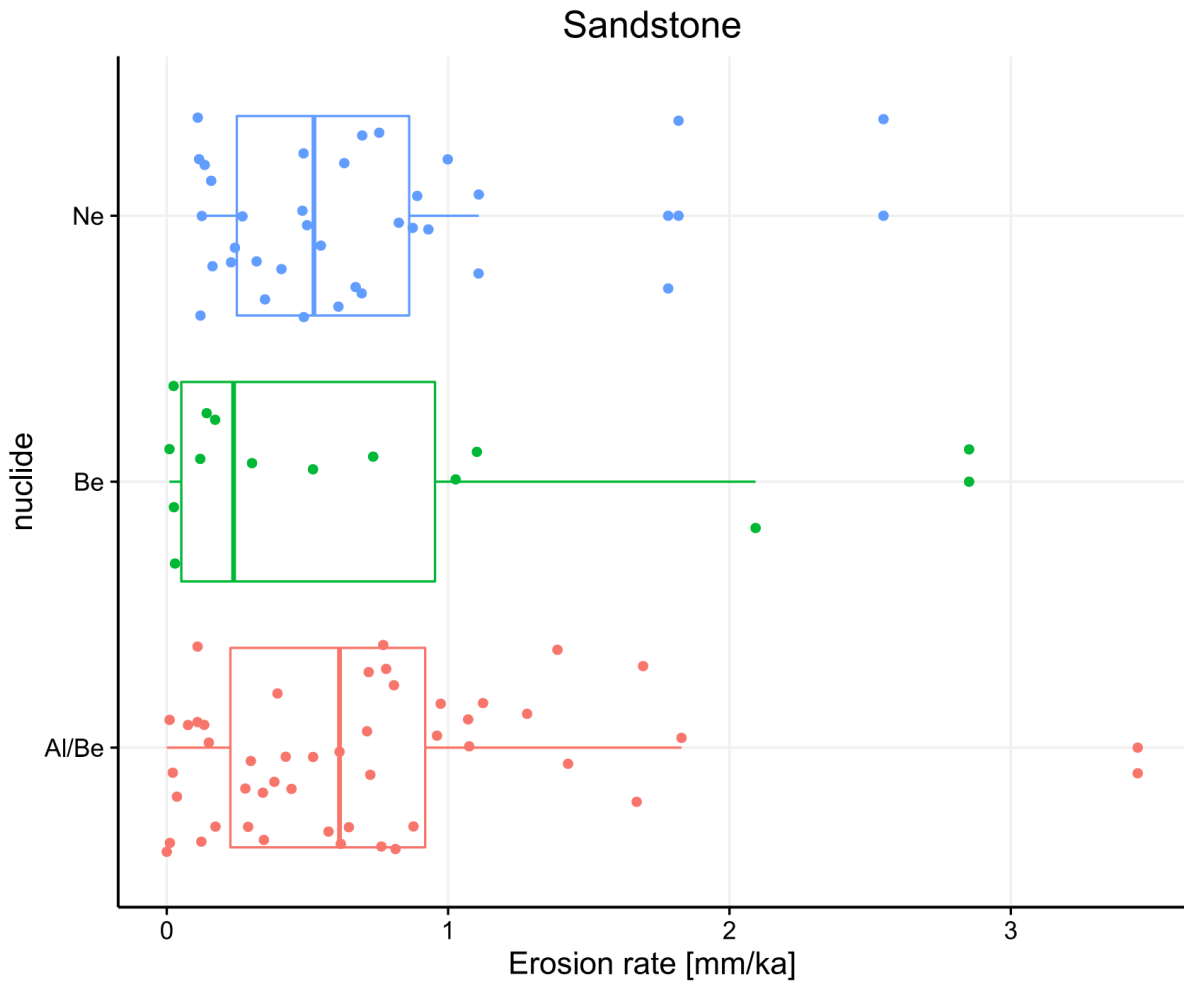

Figure S14 – Sandstone erosion rates shown for different nuclides. The groups represent 21 Ne (Ne), samples with 10Be only (Be), and samples with both 26Al and 10Be on the same sample (Al/Be).

4. Compiled References for Erosion Rate Data Set

Ackert Jr, R. P., 1999, Measurements of Past Ice Sheet Elevations in Interior West Antarctica: Science, v. 286, no. 5438, p. 276-280.

Ackert, R. P., and Kurz, M. D., 2004, Age and uplift rates of Sirius Group sediments in the Dominion Range, Antarctica, from surface exposure dating and geomorphology: Global and Planetary Change, v. 42, no. 1-4, p. 207-225.

Altmaier, M., Herpers, U., Delisle, G., Merchel, S., and Ott, U., 2010, Glaciation history of Queen Maud Land (Antarctica) reconstructed from in-situ produced cosmogenic 10Be, 26Al and 21Ne: Polar Science, v. 4, no. 1, p. 42-61.

Balco, G., and Shuster, D. L., 2009, Production rate of cosmogenic 21Ne in quartz estimated from 10Be, 26Al, and 21Ne concentrations in slowly eroding Antarctic bedrock surfaces: Earth and Planetary Science Letters, v. 281, no. 1-2, p. 48-58.

Balco, G., Stone, J. O. H., Sliwinski, M. G., and Todd, C., 2014, Features of the glacial history of the Transantarctic Mountains inferred from cosmogenic 26Al, 10Be and 21Ne concentrations in bedrock surfaces: Antarctic Science, v. 26, no. 06, p. 708-723.

Bromley, G. R. M., Hall, B. L., Stone, J. O., Conway, H., and Todd, C. E., 2010, Late Cenozoic deposits at Reedy Glacier, Transantarctic Mountains: implications for former thickness of the West Antarctic Ice Sheet: Quaternary Science Reviews, v. 29, no. 3-4, p. 384-398.

Brook, E. J., Brown, E. T., Kurz, M. D., Ackert, R. P., Raisbeck, G. M., and Yiou, F., 1995, Constraints on age, erosion, and uplift of Neogene glacial deposits in the Transantarctic Mountains determined from in situ cosmogenic 10Be and 26Al: Geology, v. 23, no. 12, p. 1063.

Brown, E. T., Edmond, J. M., Raisbeck, G. M., Yiou, F., Kurz, M. D., and Brook, E. J., 1991, Examination of surface exposure ages of Antarctic moraines using in situ produced 10Be and 26Al: Geochimica et Cosmochimica Acta, v. 55, p. 2269-2283.

Bruno, L. A., Baur, H., Graf, T., Schluchter, C., Signer, P., and Wieler, R., 1997, Dating of Sirius Group tillites in the Antarctic Dry Valleys with cosmogenic 3He and 21Ne: Earth and Planetary Science Letters, v. 147, p. 37-54.

Di Nicola, L., Baroni, C., Strasky, S., Salvatore, M. C., Schlüchter, C., Akçar, N., Kubik, P. W., and Wieler, R., 2012, Multiple cosmogenic nuclides document the stability of the East Antarctic Ice Sheet in northern Victoria Land since the Late Miocene (5–7 Ma): Quaternary Science Reviews, v. 57, p. 85-94.

Fink, D., McKelvey, B., Hambrey, M., Fabel, D., and Brown, R., 2006, Pleistocene deglaciation chronology of the Amery Oasis and Radok Lake, northern Prince Charles Mountains, Antarctica: Earth and Planetary Science Letters, v. 243, no. 1-2, p. 229-243.

Fogwill, C. J., Bentley, M. J., Sugden, D. E., Kerr, A. R., and Kubik, P. W., 2004, Cosmogenic nuclides 10Be and 26Al imply limited Antarctic Ice Sheet thickening and low erosion in the Shackleton Range for >1 m.y: Geology, v. 32, no. 3, p. 265.

Hodgson, D. A., Bentley, M. J., Schnabel, C., Cziferszky, A., Fretwell, P., Convey, P., and Xu, S., 2012, Glacial geomorphology and cosmogenic 10Be and 26Al exposure ages in the northern Dufek Massif, Weddell Sea embayment, Antarctica: Antarctic Science, v. 24, no. 04, p. 377-394.

Huang, F., Li, G., Liu, X., Kong, P., Ju, Y., Fink, D., Fang, A., and Yu, L., 2010, Minimum Bedrock Exposure Ages and Their Implications: Larsemann Hills and Neighboring Bolingen Islands, East Antarctica: Acta Geologica Sinica, v. 84, no. 3, p. 543-548.

Ivy-Ochs, S., Schluchter, C., Kubik, P. W., Dittrich-Hannen, B., and Beer, J., 1995, Minimum 10Be exposure ages of early Pliocene for the Table Mountain plateau and the Sirius Group at Mount Fleming, Dry Valleys, Antarctica: Geology, v. 23, no. 11, p. 1007-1010.

Kiernan, K., Gore, D. B., Fink, D., White, D. A., McConnell, A., and Sigurdsson, I. A., 2009, Deglaciation and weathering of Larsemann Hills, East Antarctica: Antarctic Science, v. 21, no. 04, p. 373.

Lilly, K., Fink, D., Fabel, D., and Lambeck, K., 2010, Pleistocene dynamics of the interior East Antarctic ice sheet: Geology, v. 38, no. 8, p. 703-706.

Margerison, H. R., Phillips, W. M., Stuart, F. M., and Sugden, D. E., 2005, Cosmogenic 3He concentrations in ancient flood deposits from the Coombs Hills, northern Dry Valleys, East Antarctica: interpreting exposure ages and erosion rates: Earth and Planetary Science Letters, v. 230, no. 1-2, p. 163-175.

Matsuoka, N., Thomachot, C. E., Oguchi, C. T., Hatta, T., Abe, M., and Matsuzaki, H., 2006, Quaternary bedrock erosion and landscape evolution in the Sør Rondane Mountains, East Antarctica: Reevaluating rates and processes: Geomorphology, v. 81, no. 3-4, p. 408-420.

Middleton, J. L., Ackert, R. P., and Mukhopadhyay, S., 2012, Pothole and channel system formation in the McMurdo Dry Valleys of Antarctica: New insights from cosmogenic nuclides: Earth and Planetary Science Letters, v. 355-356, p. 341-350.

Mukhopadhyay, S., Ackert, R. P., Pope, A. E., Pollard, D., and DeConto, R. M., 2012, Miocene to recent ice elevation variations from the interior of the West Antarctic ice sheet: Constraints from geologic observations, cosmogenic nuclides and ice sheet modeling: Earth and Planetary Science Letters, v. 337-338, p. 243-251.

Nishiizumi, K., Kohl, C. P., Arnold, J. R., Klein, J., Fink, D., and Middleton, J. L., 1991, Cosmic ray produced 10Be and 26Al in Antarctic rocks: exposure and erosion history: Earth and Planetary Science Letters, v. 104, p. 440-454.

Oberholzer, P., Baroni, C., Salvatore, M. C., Baur, H., and Wieler, R., 2008, Dating late Cenozoic erosional surfaces in Victoria Land, Antarctica, with cosmogenic neon in pyroxenes: Antarctic Science, v. 20, no. 01, p. 89-98.

Oberholzer, P., Baroni, C., Schaefer, J. M., Orombelli, G., Ochs, S. I., Kubik, P. W., Baur, H., and Wieler, R., 2003, Limited Pliocene/Pleistocene glaciation in Deep Freeze Range, northern Victoria Land, Antarctica, derived from in situ cosmogenic nuclides: Antarctic Science, v. 15, no. 4, p. 493-502.

Schaefer, J. M., Ivy-Ochs, S., Wieler, R., Leya, I., Baur, H., Denton, G. H., and Schluchter, C., 1999, Cosmogenic noble gas studies in the oldest landscape on earth: surface exposure ages of the Dry Valleys, Antarctica: Earth and Planetary Science Letters, v. 167, p. 215-226.

Staiger, J. W., Marchant, D. R., Schaefer, J. M., Oberholzer, P., Johnson, J. V., Lewis, A. R., and Swanger, K. M., 2006, Plio-Pleistocene history of Ferrar Glacier, Antarctica: Implications for climate and ice sheet stability: Earth and Planetary Science Letters, v. 243, no. 3-4, p. 489-503.

Summerfield, M. A., Sugden, D. E., Denton, G. H., Marchant, D. R., Cockburn, H. A. P., and Stuart, F. M., 1999, Cosmogenic isotope data support previous evidence of extremely low rates of denudation in the Dry Valleys region, southern Victoria Land, Antarctica: Geological Society, London, Special Publications, v. 162, no. 1, p. 255-267.

Swanger, K. M., Marchant, D. R., Schaefer, J. M., Winckler, G., and Head, J. W., 2011, Elevated East Antarctic outlet glaciers during warmer-than-present climates in southern Victoria Land: Global and Planetary Change, v. 79, no. 1-2, p. 61-72.

White, D. A., Bennike, O., Berg, S., Harley, S. L., Fink, D., Kiernan, K., McConnell, A., and Wagner, B., 2009, Geomorphology and glacial history of Rauer Group, East Antarctica: Quaternary Research, v. 72, no. 1, p. 80-90.

5. Notes on Excluded Samples

There were originally 283 individual analyses extracted from the literature. For various reasons outlined below, 55 analyses were removed. Condensed samples by averaging duplicate analyses on the same sample using the same nuclide and removed 34 samples. The total number of analyses used in the final compilation: 194.

Removed samples:

Missing information (4): Bruno 1997 (2), Huang 2010 (2)
Negative erosion (2): Altmaier 2010 (1), Brook 1995 (1)
He in quartz (19): Brook 1995 (2), Brown 1991 (17)
Ne in pyroxene (16): Oberholzer 2008 (6), Schaefer 1999 (10),
Complex exposure (Al/Be outlier) (4): Fogwill 2004 (2), Brook 1995 (1), Nishiizumi 1991 (1)
Not saturated data (4): Ackert 1999 (4)
Concentrations not given for Ne (6): Schaefer 1999 (Ne in quartz)

6. Compiled Data Set - Individual Discussion

6.1. **Elevation** The elevation of each sample was taken from the original publications. When plotted against elevation, as in Figure S15, there is no significant trend in erosion rate. This is not unexpected due to the lack of elevational trends in other variables that sometimes covary with elevation, such as precipitation or temperature. The highest erosion rates do occur at the lower elevations; however, low erosion rates occur at all elevations. There are no high erosion rates recorded at high elevations. Possible explanations for these trends include true differences in erosional regime due to different glacial histories at different elevations, artificially inflated erosion rates due to more cold-based/non-erosive burial at lower elevations, and lack of large numbers of samples at high elevations leading to unrepresentative reported erosion rates. Relative elevation above ice might provide better insight into possible elevation trends, but this is unavailable for many studies and is difficult to recreate in a consistent/automated manner for individual samples.

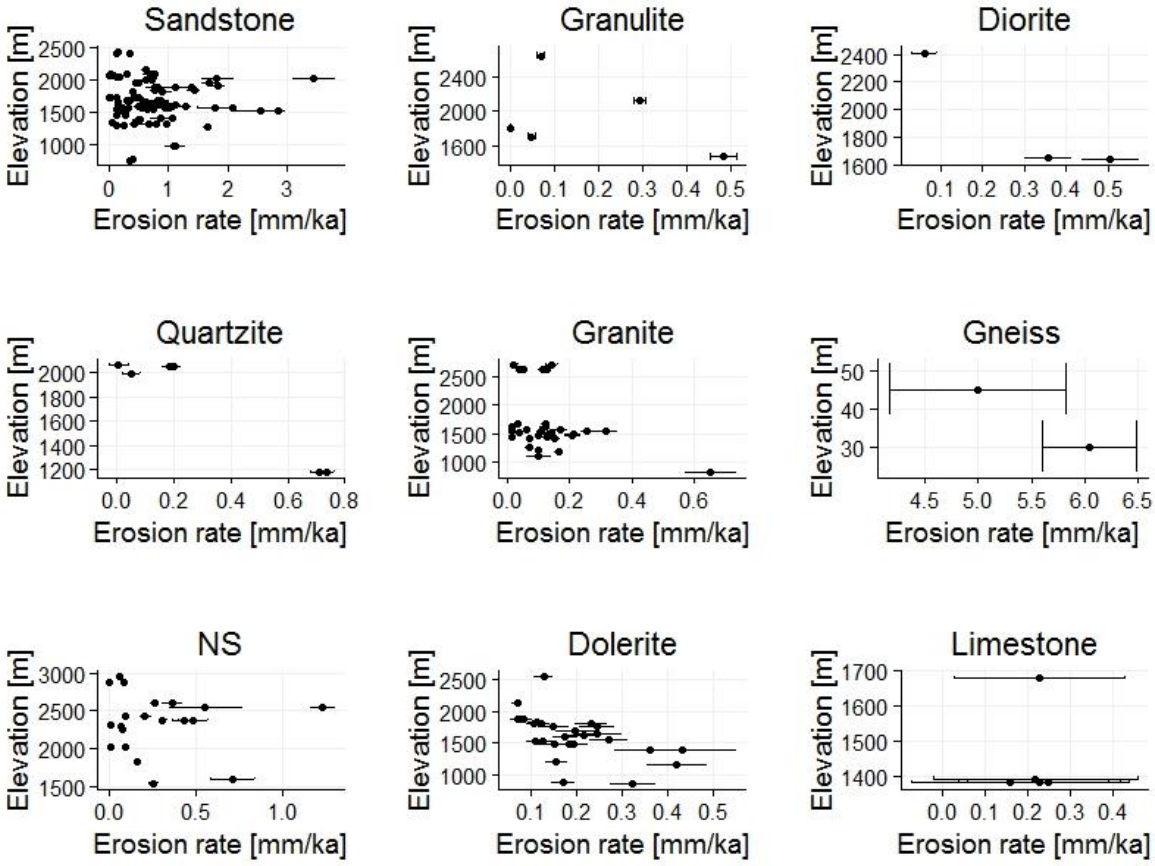

Figure S15: Erosion rate plotted for each rock type. NS indicates all samples where lithology was not specified.

6.2. **Publication Year** If sample measurement techniques improved or changed through the years, a trend in erosion rates might be expected to covary. However, no trend in erosion rate is seen when plotted according to publication year.

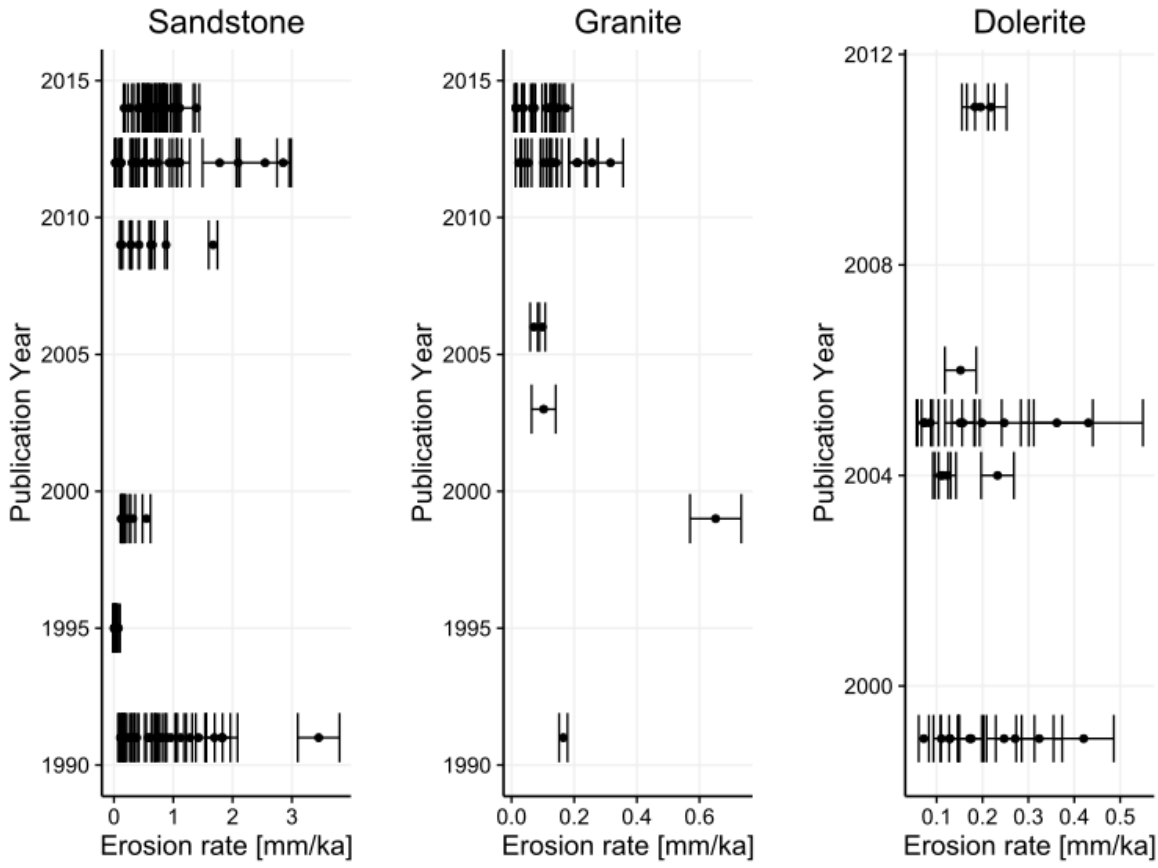

Figure S16: Erosion rates by publication year, separated by lithology. Shown only for lithologies with statistically significant numbers of samples.

6.3. Coastal Location Samples were divided into either coastal or interior locations, with 'coastal locations' being defined as any sample within ~50km of the coast. Samples in the Dry Valleys were classified as 'coastal' and make up the vast majority of the coastal samples. With only eleven non-Dry Valleys coastal samples, there are not a statistically significant number of these to compare with the interior samples to determine if there are any significant trends (Figure S17). The larger spread of Dry Valleys samples compared to other locations is discussed in the main text.

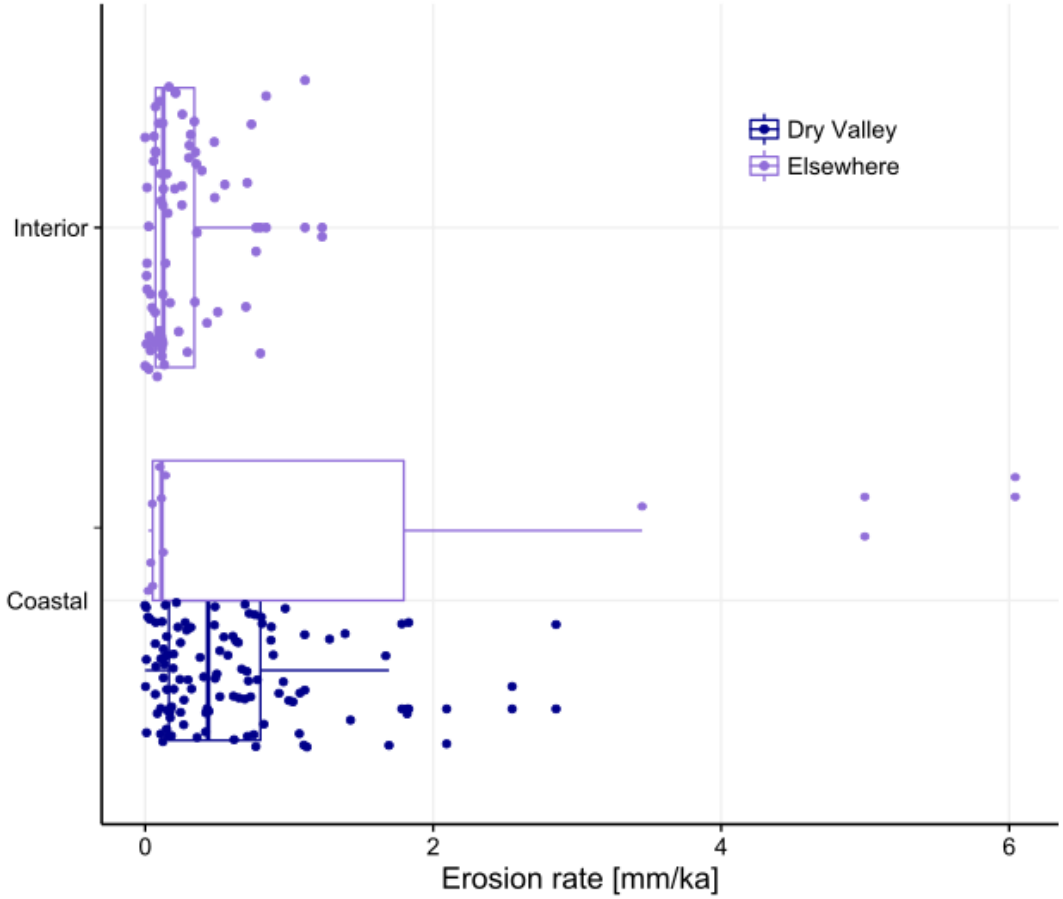

Figure S17: Erosion rates for coastal and interior samples, with samples from the Dry Valleys separated out from other coastal locations.

6.4. Log normal distributions Samples within each lithology are skewed towards a significant number of samples with lower erosion rates. For some analyses and comparisons, it can be necessary to work with the data in log space (Portenga and Bierman, 2011). Once converted to log(10), the distributions are generally log normal within each lithology (Figure S18) and also within other subsections, like boulders and bedrock (Figure S19). To avoid this, we have chosen to report quartiles of the data instead of standard deviation or other statistics that require this type of conversion.

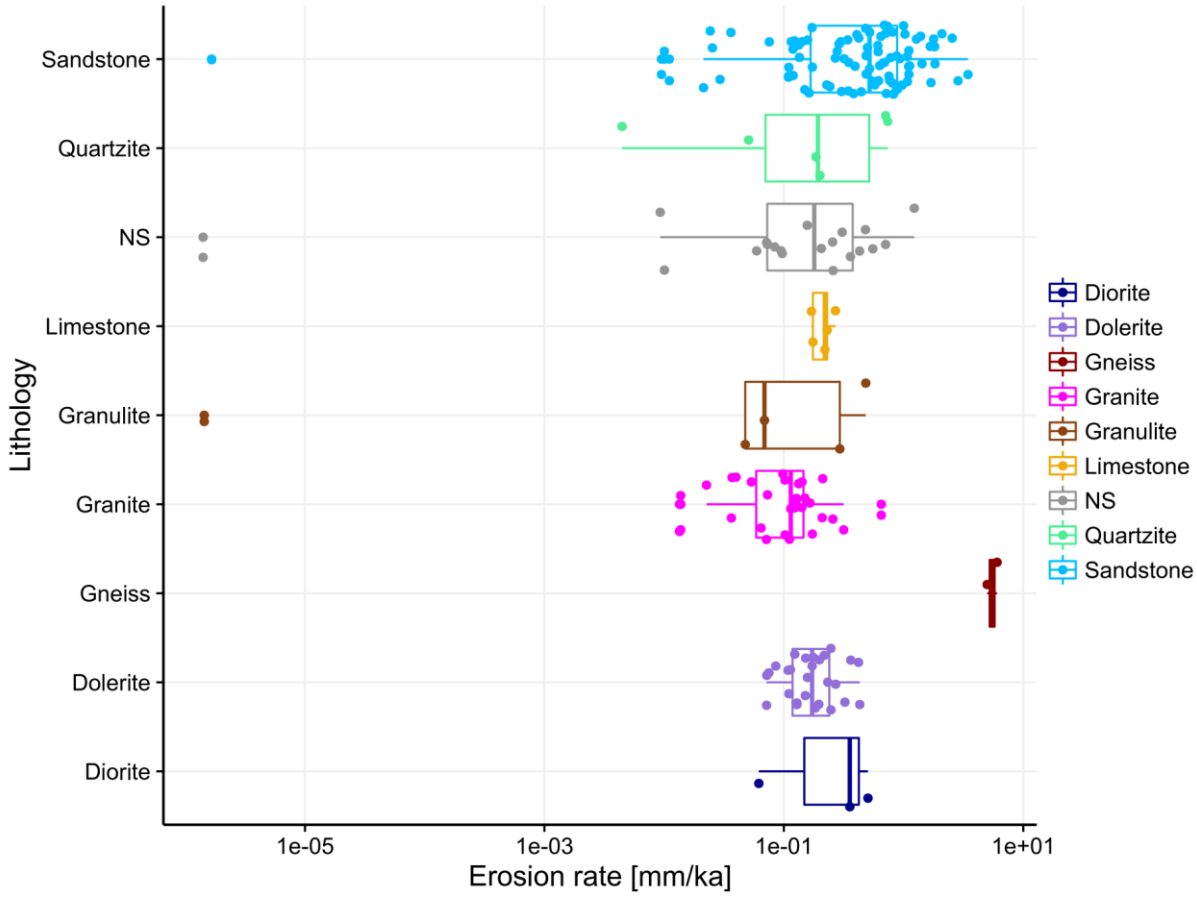

Figure S18: Erosion rates viewed in log(10) space for each lithology.

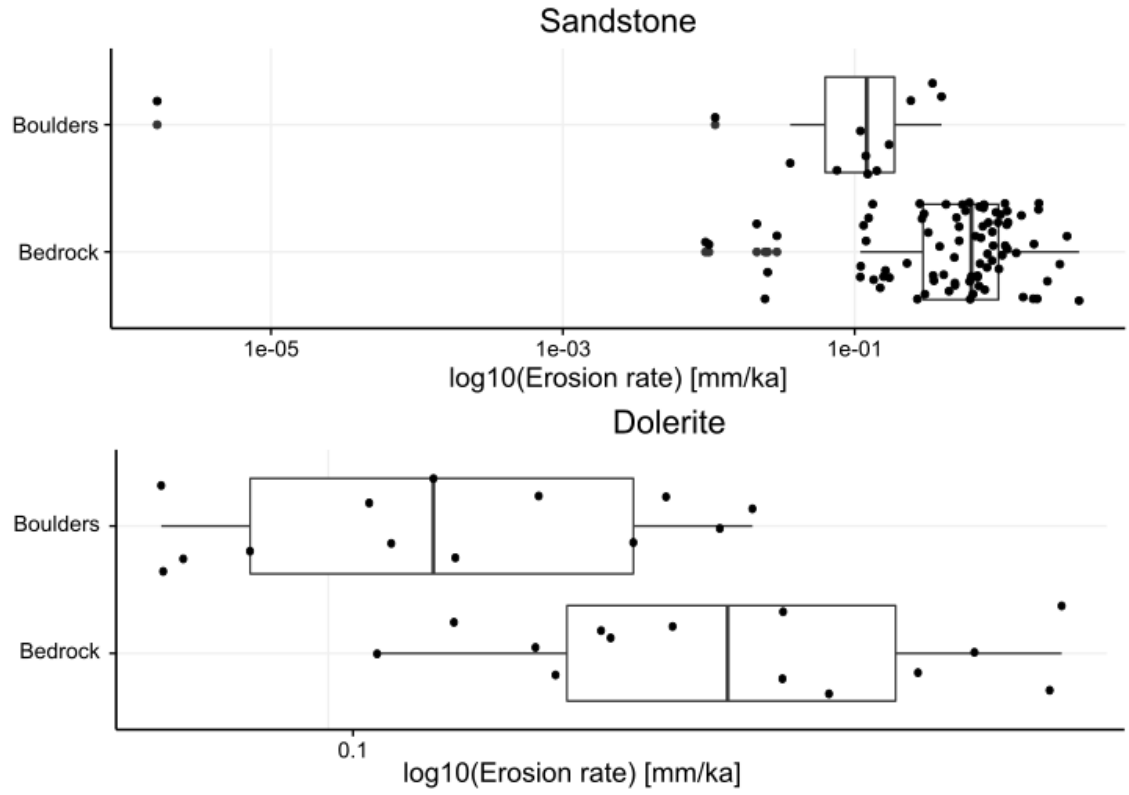

Figure S19: Erosion rates viewed in log(10) space for boulder and bedrock populations for sandstone and dolerite.

6.5. Individual studies Although there are systematic differences in the results from some studies, the removal of any one study does not affect the general conclusions drawn here. As an example, the erosion rates for sandstone are shown broken down by study in Figure S20.

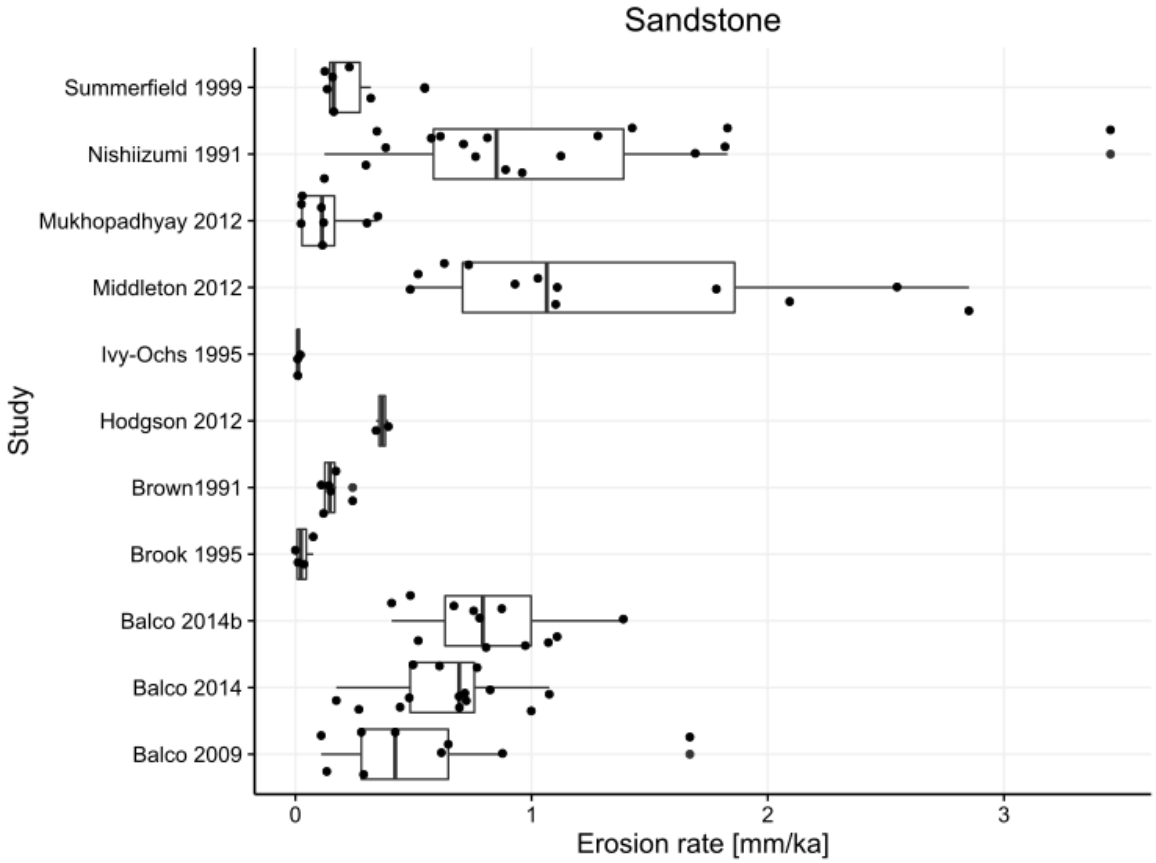

Figure S20: Erosion rates for sandstone broken down by individual study. Full references for studies can be found in Section 4.

6.6. Effect of the Dry Valleys The main paper discusses the fact that the Dry Valleys seems to show higher erosion rates compared to elsewhere on the continent. This is presented in general in the main paper and Table S1 presents the relevant statistics (Mean, Median, First Quartile, and Third Quartile) for all lithologies represented in the Dry Valleys and Elsewhere. While there are some groups with a smaller number of samples than might be ideal for drawing large-scale conclusions, the general conclusions are supported by the smaller number of data points. For example, although the mean/median of sandstone is much closer to that of dolerite and granite outside of the Dry Valleys, the spread of the data is still much larger than the other lithologies, consistent with the overall dataset.

	All				Dry Valleys				Elsewhere			
	1st	**Med**	**Mean**	**3rd**	**1st**	**Med**	**Mean**	**3rd**	**1st**	**Med**	Mean	3rd
Dolerite	0.12	0.17	0.19	0.24	0.13	0.18	0.20	0.25	0.11	0.12	0.14	0.15
Granite	0.06	0.11	0.13	0.15	0.65	0.65	0.65	0.65	0.06	0.11	0.11	0.14
Quartzite	0.08	0.19	0.31	0.58	0.09	0.19	0.13	0.19	0.38	0.71	0.50	0.72
Sandstone	0.17	0.52	0.67	0.88	0.25	0.62	0.70	0.95	0.11	0.12	0.44	0.35

Table S1: Relevant statistics for comparisons of erosion rates within and outside of the Dry Valleys. Values shown are Mean, Median, First Quartile, and Third Quartile for all lithologies represented both in the Dry Valleys and elsewhere.

6.7. Temperature The comparison of erosion rates and temperature did not show a significant trend. The highest erosion rates occur at approximately -40 degrees C, but this is the range for many of the Dry Valleys samples and temperature does not seem to be a distinguishing factor (see main paper discussion).

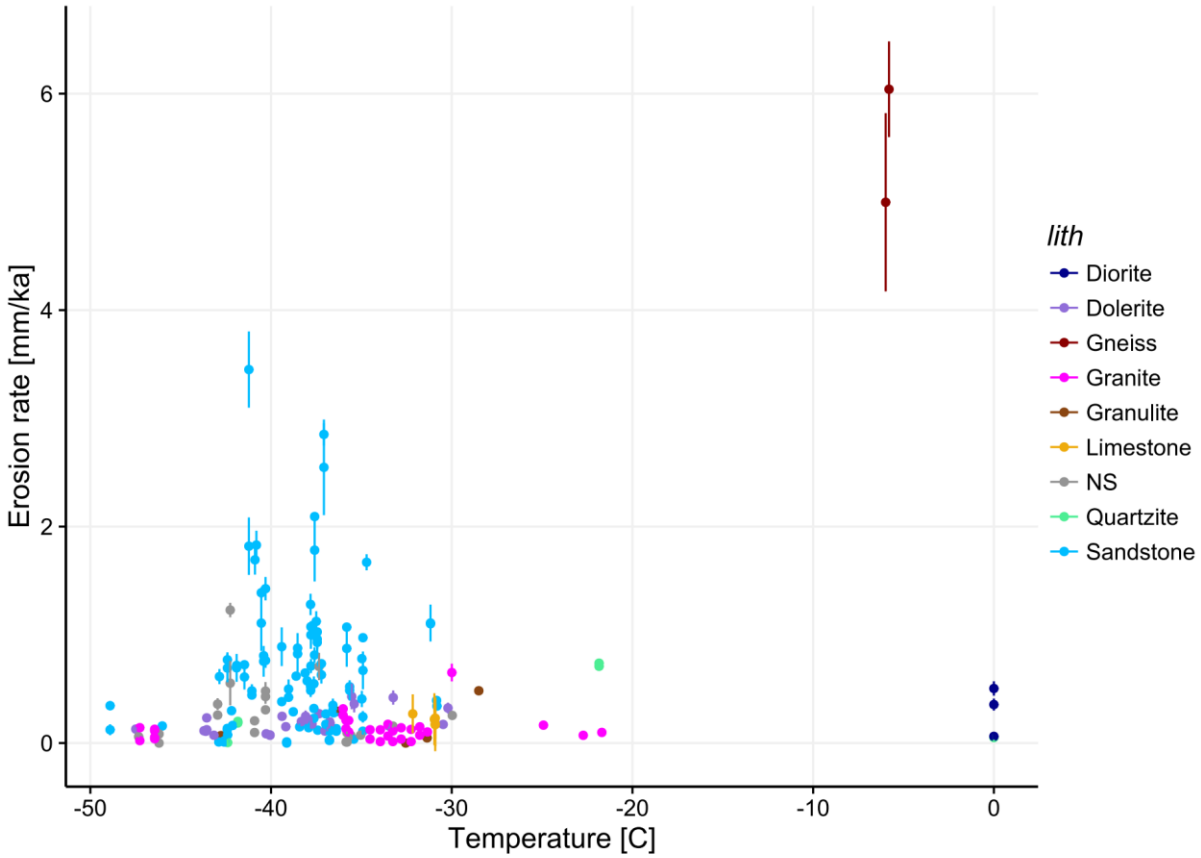

Figure S21 – Erosion rates plotted against temperature, broken down by lithology.

6.8. Latitude There is no significant trend in erosion rates when plotted against latitude. Once again, samples from the Dry Valleys are clearly distinguishable from the others (samples at approximately -80 latitude).

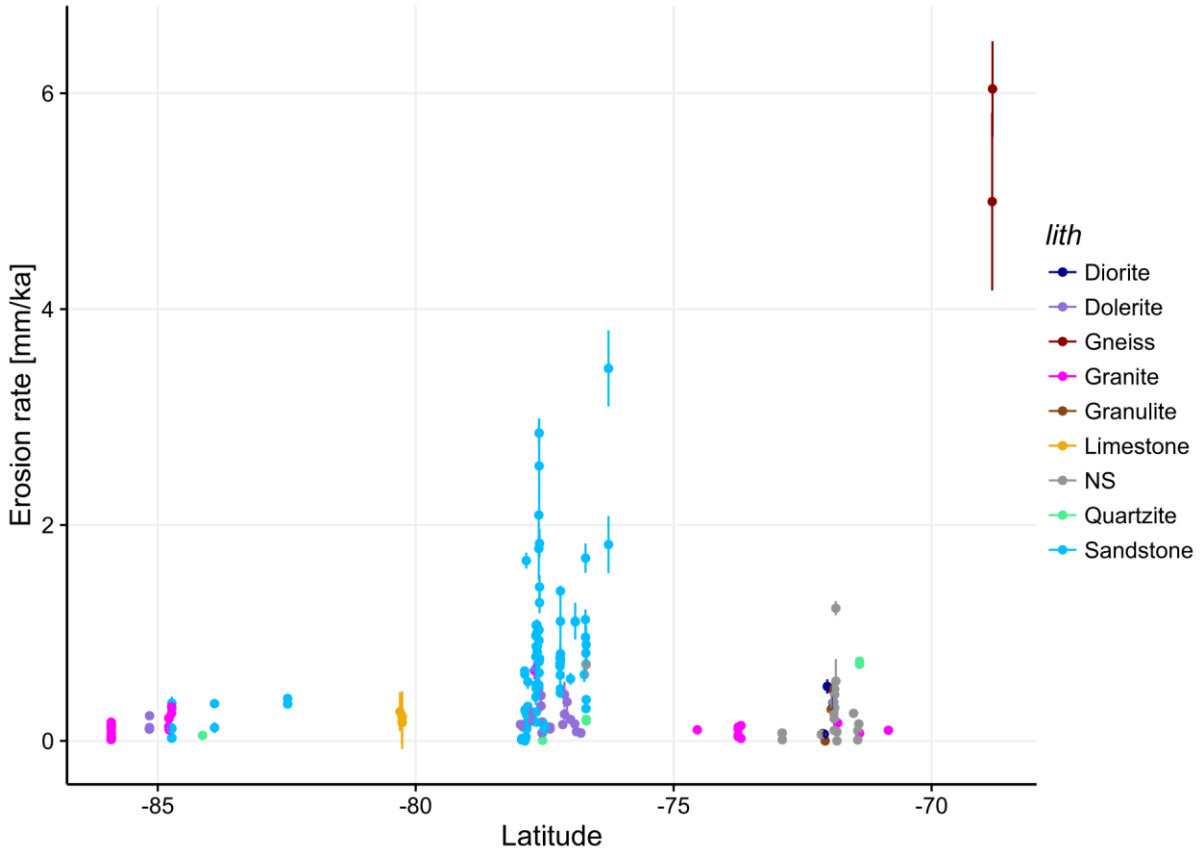

Figure S22 – Samples erosion rates plotted against latitude, broken down by lithology.

Supplemental References

Amidon, W. H., Rood, D. H., and Farley, K. A., 2009, Cosmogenic 3He and 21Ne production rates calibrated against 10Be in minerals from the Coso volcanic field: Earth and Planetary Science Letters, v. 280, no. 1-4, p. 194-204.

Balco, G., and Shuster, D. L., 2009, Production rate of cosmogenic 21Ne in quartz estimated from 10Be, 26Al, and 21Ne concentrations in slowly eroding Antarctic bedrock surfaces: Earth and Planetary Science Letters, v. 281, no. 1-2, p. 48-58.

Borchers, B., Marrero, S., Balco, G., Caffee, M., Goehring, B. M., Gosse, J., Lifton, N., Nishiizumi, K., Phillips, F. M., Schaefer, J., and Stone, J. O., 2016, Geological calibration of spallation production rates in the CRONUS-Earth project: Quaternary Geochronology, v. 31, p. 188-198.

Dunai, T. J., 2010, Cosmogenic Nuclides: Principles, Concepts and Applications in the Earth Surface Sciences, Cambridge, Cambridge University Press, 187 p.

Faure, G., 1987, Principles of Isotope Geology, 2nd Edition. John Wiley & Sons, 589 pp. ISBN 0-471-86412-9.

Lal, D., 1991, Cosmic ray labeling of erosion surfaces: In situ nuclide production rates and erosion models: Earth and Planetary Science Letters, v. 104, p. 424-439.

Lifton, N., Sato, T., and Dunai, T. J., 2014, Scaling in situ cosmogenic nuclide production rates using analytical approximations to atmospheric cosmic-ray fluxes: Earth and Planetary Science Letters, v. 386, p. 149-160.

Marrero, S., Phillips, F., Caffee, M., and Gosse, J., 2016, CRONUS-Earth cosmogenic ^{36}Cl calibration: Quaternary Geochronology, v. 31, p. 199-219.

Niedermann, S., Graf, T., Kim, J. S., Kohl, C. P., Marti, K., and Nishiizumi, K., 1994, Cosmic-ray produced ^{21}Ne in terrestrial quartz: the neon inventory of Sierra Nevada quartz separates: Earth and Planetary Science Letters, v. 125, p. 341-355.

Phillips, F. M., Argento, D. C., Balco, G., Caffee, M. W., Clem, J., Dunai, T., Finkel, R., Goehring, B., Gosse, J. C., Hudson, A., Jull, T. A., Kelly, M., Kurz, M., Lal , D., Lifton, N., Marrero, S. M., Nishiizumi, K., Reedy, R., Schaefer, J., Stone, J. O., Swanson, T., and Zreda, M. G., 2016, The CRONUS-Earth Project: A synthesis: Quaternary Geochronology, v. 31, p. 119-154.

Portenga, E. W., and Bierman, P. R., 2011, Understanding Earth's eroding surface with 10Be: GSA Today, v. 21, no. 8, p. 4-10.

Vermeesch, P., Baur, H., Heber, V. S., Kober, F., Oberholzer, P., Schaefer, J. M., Schlüchter, C., Strasky, S., and Wieler, R., 2009, Cosmogenic 3He and 21Ne measured in quartz targets after one year of exposure in the Swiss Alps: Earth and Planetary Science Letters, v. 284, no. 3-4, p. 417-425.

Wilcken, K. M., Freeman, S. P. H. T., Schnabel, C., Binnie, S. A., Xu, S., and Phillips, R. J., 2013, 36Cl accelerator mass spectrometry with a bespoke instrument: Nuclear Instruments and Methods in Physics Research Section B: Beam Interactions with Materials and Atoms, v. 294, p. 107-114.